RESEARCH ARTICLE

NANO · MICRO small
www.small-journal.com

Engineering Autologous Cell-Derived Exosomes to Boost Melanoma-Targeted Radio-Immunotherapy by Cascade cGAS-STING Pathway Activation

Fangming Zhang, Ziyao Zhang, Wanting Yang, Zhuyuan Peng, Juntao Sun, Guofeng Li, Yen Wei, Xing Wang, Lingyun Zhao,* and Wensheng Xie**

Radio-immunotherapy has offered emerging opportunities to treat invasive melanoma due to its immunostimulatory performances to activate antitumor immune responses. However, the immunosuppressive microenvironment and insufficient response rate significantly limit the practical efficacy. This study presents an autologous cell-derived exosomes (Exo)-engineered nanoagonist (MnExo@cGAMP) containing with metalloimmunotherapeutic agent (Mn^{2+} ions) and nucleotidyltransferase (2′,3′-cGAMP, a STING agonist) for boosting melanoma-targeted radio-immunotherapy by cascade cGAS-STING pathway activation. The MnExo@cGAMP can efficiently accumulate in tumor cells due to the autologous targeting performance. Once internalized by tumor cells, the released Mn^{2+} ions will enhance stimulator of interferon gene (STING) binding and sensitize cyclic GMP-AMP (cGAS) to radiotherapy-induced double-straned DNA (dsNDA), resulting in amplification of cGAS-STING pathway activation together with X-ray irradiation. Meanwhile, loaded 2′,3′-cGAMP can directly augment pathway activity acting as a secondary messenger. These cascade activations of cGAS-STING pathway trigger the overexpression of type I interferon, promote dendritic cells (DCs) maturation, antigen presentation, and increase $CD8^+$ T cell activation, resulting effective radio-immunotherapeutic outcome by overcoming immune-suppression in melanoma. This study demonstrates a targeted therapeutic modality involving metalloimmunotherapy and agonist for efficient melanoma radio-immunotherapy by cascade cGAS-STING pathway activation.

1. Introduction

Melanoma is the most lethal skin cancer which originates from the malignant transformation of melanocytes.[1] The incidence of melanoma around the world is about 1.7% of all new-diagnosed primary malignant cancer and mortality is ≈0.7%.[2] Currently, surgery, radiotherapy, targeted therapies for V-Raf murine sarcoma viral oncogene homolog inhibition and immunotherapies have main clinical strategies for melanoma patients.[3,4] However, the low response rate and inevitable occurrence of resistance still greatly limit the prognosis improvement due to the immunosuppressive tumor environment, cytotoxic resistance by immune cells, and developed lesions in antigen process.[1,5,6] Meanwhile, although melanoma is one of the most immunogenic tumors, the intrinsic plasticity allows it evade the immunosurveillance and escape immune response during the radiotherapy.[7] Therefore, it is of great significance to develop novel strategy for blocking immune escape and improving therapeutic outcome.

Stimulator of interferon gene (STING), an intracellular signaling receptor for innate immune pathway, is critical for the initiation of antitumor immunity.[8] Preclinical studies have demonstrated that both endogenous signaling pathway and exogenous agonist STING activation could effectively arouse the adaptive immune recognition.[9,10] For instance, intratumoral injection of the natural ligands (cyclic dinucleotides, CDNs) for STING, has shown remarkable efficacy in preclinical studies and is under investigation in

F. Zhang, Z. Zhang, W. Yang, Z. Peng, J. Sun, G. Li, X. Wang, W. Xie
State Key Laboratory of Organic-Inorganic Composites
College of Life Science and Technology
Beijing University of Chemical Technology
Beijing 100029, P. R. China
E-mail: wangxing@buct.edu.cn; xws@mail.buct.edu.cn

Y. Wei
The Key Laboratory of Bioorganic Phosphorus Chemistry & Chemical Biology (Ministry of Education)
Department of Chemistry
Tsinghua University
Beijing 100084, P. R. China

L. Zhao
State Key Laboratory of New Ceramics and Fine Processing
School of Materials Science and Engineering
Tsinghua University
Beijing 100084, P. R. China
E-mail: lyzhao@mail.tsinghua.edu.cn

The ORCID identification number(s) for the author(s) of this article can be found under https://doi.org/10.1002/smll.202408769

DOI: 10.1002/smll.202408769

human clinical trials.[11] Moreover, previous study has demonstrated that combined STING activator could overcome the radiotherapy resistance during pancreatic cancer treatment.[12] Meanwhile, more CDN-based STING agonists are currently undergoing clinical trials (NBTTXR-3, idronoxil, exoSTING, IMSA-101, ADU-S100, MK-1454, TAK-676, SB-11285, SYN-STING, GSK-3745417, BI-1387446, E-7766, SNX-281, BMS-986301, and CB-85247).[13,14] However, most CDN-based STING agonists are hydrophilic small molecules, membrane impermeable and susceptible to rapid degradation by nucleases, making them unsuitable as agents for systemic administration. To address these limitations, nanotechnology is employed to endow molecule with nano-size to avoid quick degradation, increase blood circulation time, improve membrane permeability, and promote targeted cumulation, such as polymetric STING activating nanoparticles (polySTING),[15] STING-activating nano-liposomal vesicles (SAProsomes),[16] drug-conjugated poly(β-amino ester) nanoparticle formulations (CDN-NPs),[17] cyclic dimeric adenosine monophosphate-loaded nanoscale coordination polymers (ZnCDA), universal STING mimic lipid nanoparticles (LNP-uniSTING-mRNA),[18] and etc. Nanoparticle-based delivery systems effectively improve the pharmacokinetics and therapeutic efficacy. Nevertheless, relevant side effects caused by cytotoxicity of external synthetic nanoparticle components, undesired biodistribution, and poor intracellular permeation have become urgent limitations in practical application.

In addition to synthetic nanocarriers, cell-derived extracellular vesicles have attracted considerable attention as drug delivery systems due to low immunogenicity, excellent stability and biosafety, decreased immune clearance, and active targeting performances.[19,20] Particularly, exosomes, which are small extracellular vesicles of endosomal origin released by the exocytosis of multivesicular bodies and amphisomes, exhibit significant potential for cancer diagnosis and therapy for intrinsic cell-to-cell communication locally and between organs.[21,22] Moreover, exosomes can influence the proliferation and respective activity of recipient cells of innate immune system via delivery of DNA-inducing cyclic GMP-AMP (cGAS)-STING signaling and transfer and presentation of antigen peptides.[23,24] Therefore, as an autologously safe delivery vehicle, we speculate that engineered exosomes with special functions can reverse the immune escape of melanoma treatment.

Activation of cGAS-STING pathway for melanoma immunotherapy is guided by two key proteins: cGAS and STING.[25] Therefore, in this study, autologously cell-derived exosome was engineered with cyclic dinucleotides (2′,3′-cGAMP) and metalloimmunoagonists (Mn^{2+} ions) (MnExo@cGAMP) to activate the immune response of melanoma via activation of both cGAS and STING, and improve the therapeutic outcome by combining with radiotherapy (**Scheme 1**). In MnExo@cGAMP system, exosome provides efficient loading capacity, targeted delivery performance, and excellent biocompatibility. Mn^{2+} ions enhance STING bingding activity and sensitize cGAS to radiotherapy-induced dsDNA, and then intensify the cGAS-STING pathway activation together with 2′,3′-GAMP. Meanwhile, external radiation could further enhances the generation of IFN-γ, which forwardly promote dendritic cells (DCs) muturation, antigen presentation, T cell activation, and final antitumor immunity. This engineered autogolous exosomes demonstrated an unique potential to overcome the low response rate of melanoma radioimmunotherapy.

2. Results and Discussion

2.1. Rational Design and Characterization of the MnExo@cGAMP

As shown in **Figure 1**a, melanoma B16F10 cell-derived exosomes were obtained via classic gradient ultracentrifugation method[27] and then the engineered MnExo@cGAMP exosomes were prepared by sonication strategy[28] to load the 2′,3′-cGAMP and Mn^{2+} ions. Finally, membrane extrusion (0.22 μm) was employed to uniform the size distribution of as-prepared MnExo@cGAMP exosomes. The isolation protocol of autologous cell derived exosomes form B16F10 cells consists of three centrifugations with different speed to ensure the high purification (Figure 1b). The typical structure of MnExo@cGAMP exosomes was measured using high-resolution transmission electron microscopy (HRTEM) after negative staining with uranium acetate solution. Clear phospholipid bilayer membrane structure revealed the successful synthesis process and intact morphology after sonication treatment (Figure 1c). The dynamic diameter was ≈72.44 ± 17.18 nm as measured by dynamic light scattering (Figure 1d), which is consistent with image of HRTEM. Meanwhile, the symbolic proteins of Exo (TSG101 and CD81) were detected by western-blot analysis (Figure S1, Supporting Information). The results demonstrated that sonication process do not damage the integrality of Exo. Compared to naked Exo, drugs-loaded MnExo@cGAMP displayed slightly increased dynamic diameter (64.59 to 72.9 nm) and none zeta potential difference (Figure S2, Supporting Information). Furthermore, element mapping analysis on HRTEM was used to obviously exhibit the components of MnExo@cGAMP exosomes. Element N, O, and P represent exosome and loaded 2′,3′-cGAMP, while Mn reveals the Mn^{2+} ions capsulation. Results from inductively coupled plasma optical emission spectrometry (ICP-OES) measurement demonstrated that the loading rate of Mn^{2+} ions in MnExo@cGAMP exosomes was ≈5.5%. Meanwhile, the loading rate of 2′,3′-cGAMP was ≈2.69%.

2.2. In Vitro Cytotoxicity of MnExo@cGAMP Exosomes

As Manganese is critical for both cellular metabolism and cGAS-STING-mediated antitumor immune response.[26] First, the in vitro cytotoxicity to B16F10 cell line of free Mn^{2+} ions and 2′,3′-cGAMP was studied via co-incubation method. High concentration of Mn^{2+} ions exhibited dose-dependent cytotoxicity with a half maximal inhibitory concentration (IC50) of ≈102.5 μM (**Figure 2**a). When administrated Mn^{2+} ions were less than 7.5 μM (5 μM was chosen to following study), there was negligible direct cytotoxicity, which would guarantee the limited adverse effect to normal cell during antitumor treatment. 2′,3′-cGAMP did not show cytotoxicity to B16F10 cells even with a high concentration of 80 μM (Figure 2b). It should be noted that naked exosomes exhibited excellent biocompatibility and in vitro cytotoxicity of MnExo and MnExo@cGAMP exosomes was originated from

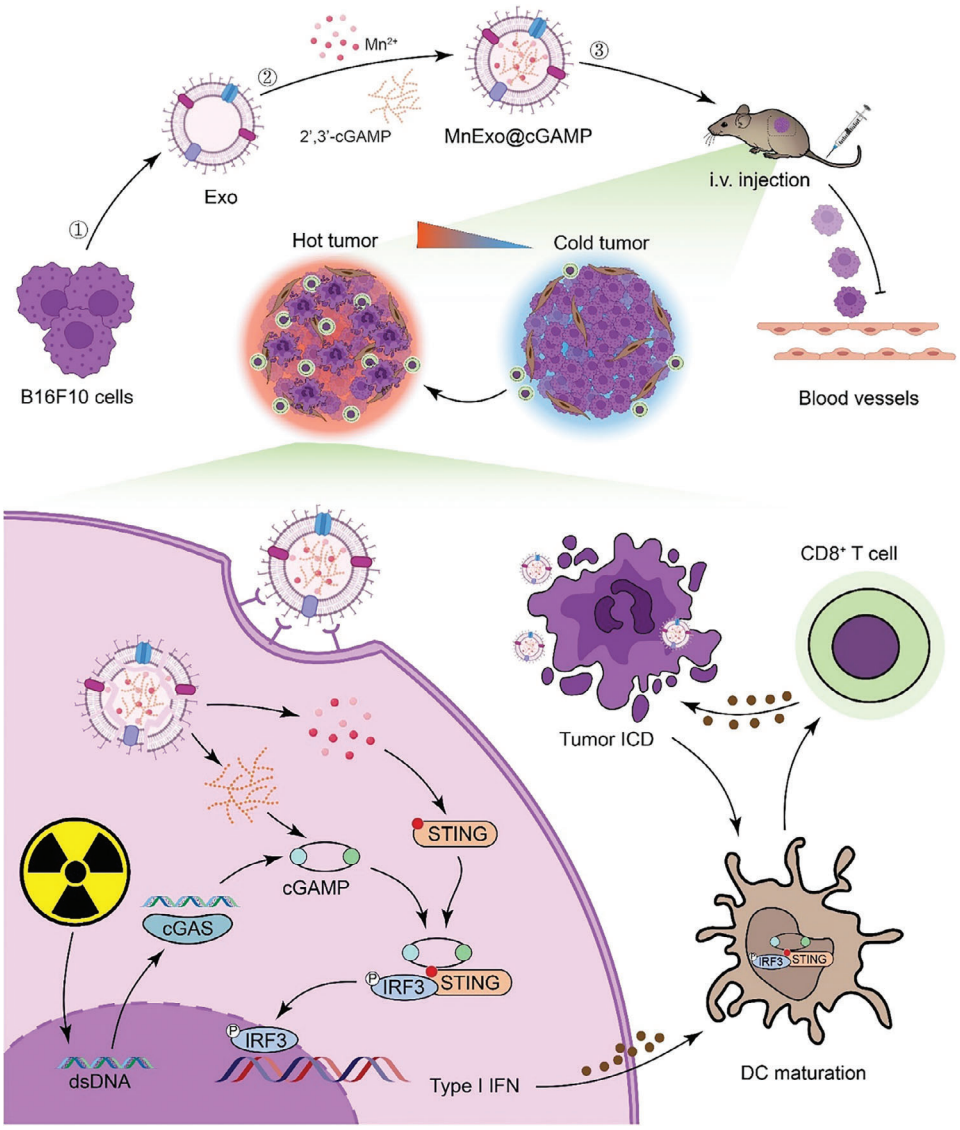

Scheme 1. The design of engineered homologous cell derived exosomes loading with immunoagonists (Mn^{2+} ions and 2′,3′-cGAMP) to transform "cold tumor" into "hot tumor" for bossting immunotherapy efficacy of melanoma.[26] In this system, released Mn^{2+} ions will sensitize cGAS to irradiation induced dsDNA for cGAMP synthesis together with released 2′,3′cGAMP. Mn^{2+} also enhance the binding of STING and cGAMP, and then activate the cGAS-STING pathway in both tumor cells and DCs, resulting in boosting antitumor immunity.

loaded Mn^{2+} ions (Figure 2c). In order to maximize the therapeutic side effect, the formulation of MnExo@cGAMP (100 μg mL^{-1}) was chosen in the following evaluation. Cell cloning experiment was used to test the sensitivity of B16F10 cells to various dose of X-ray irradiation. As shown in Figure 2d,e, few clone were observed once the irradiation dose was more than 6 Gy, demonstrating the significant therapeutic efficacy of radiotherapy to melanoma.[29,30]

It is well-known that high concentration of Mn^{2+} ions would cause the cellular apoptosis and/or pyroptosis.[31–33] The flow cytometry results (Figure 2f,g) revealed that late apoptosis varied for MnExo and MnExo@cGAMP exosomes co-incubated cells compared to the Control group and Exo group. Meanwhile, early apoptotic cells appeared in all groups, indicated that higher concentration of autologous cell-derived exosomes could cause the source cell apoptosis.[34] Furthermore, the cell cycle of treated B16F10 cells was analyzed by flow cytometry to identify phase state. As shown in Figure 2h,i, the numbers of S phase decreased and G_0/G_1 phase increased in MnExo and MnExo@cGAMP exosomes-treated groups compared to the Control and Exo group, indicated that MnExo@cGAMP caused the G_0/G_1 cell cycle arrest.

2.3. DCs Maturation, Antigen Presentation and T Cell Activaition

DCs paly an essential role for antitumor innate immune responses for its key process of antigen presentation.[35] Moreover,

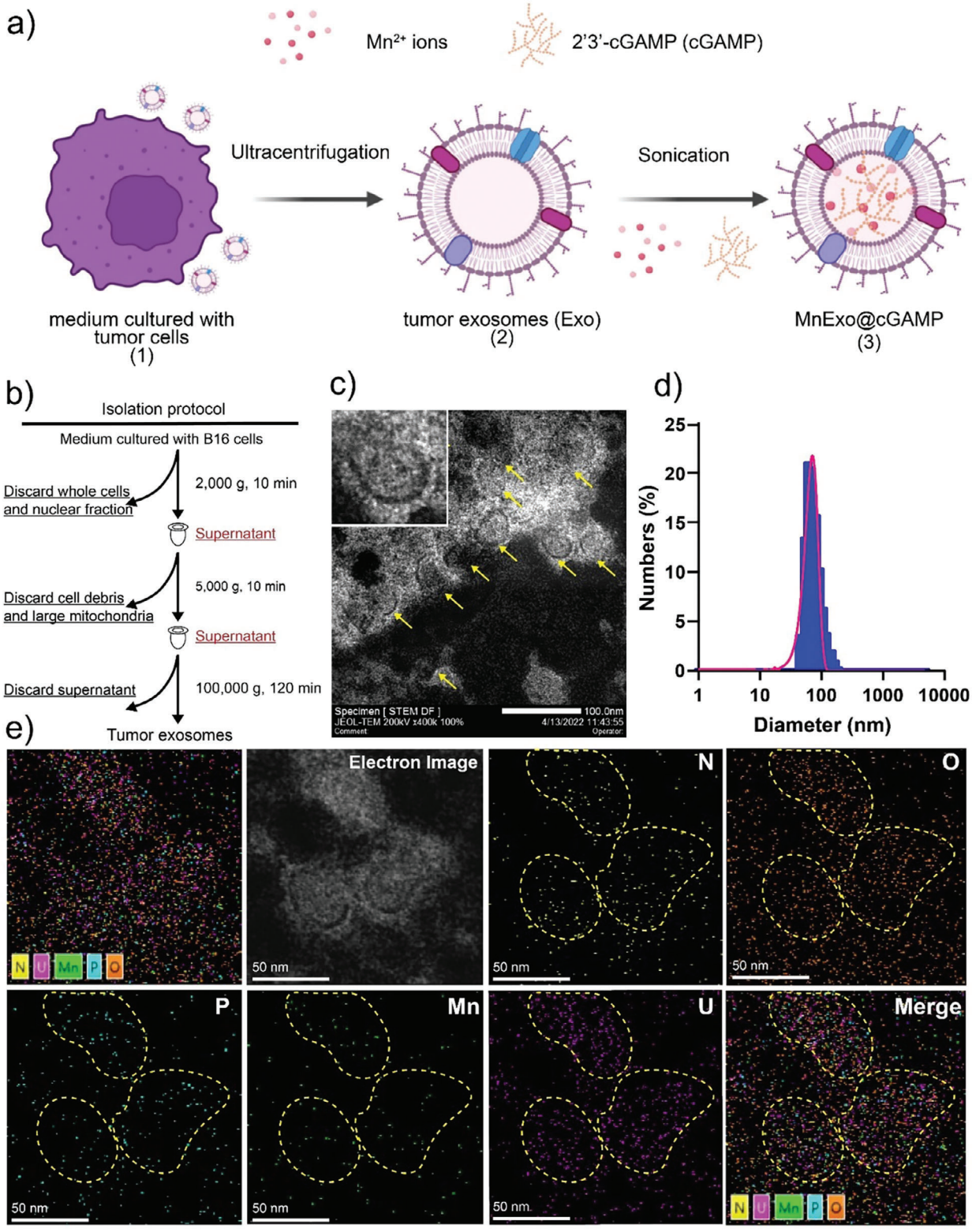

Figure 1. Preparation and characterization of engineered homologous cell-derived exosomes (MnExo@cGAMP). a) Schematically illustrating the synthetic process of MnExo@cGAMP. b) The isolation protocol to separate tumor exosome from B16F10 cells via high-speed centrifugation. c) TEM images of synthesized MnExo@cGAMP after negative staining with uranium acetate solution. d) Dynamic light scattering analysis of MnExo@cGAMP for hydrodynamic size distribution in PBS. e) TEM image and corresponding element mappings of N (yellow), O (brown), P (cyan), Mn (green), and U (pink).

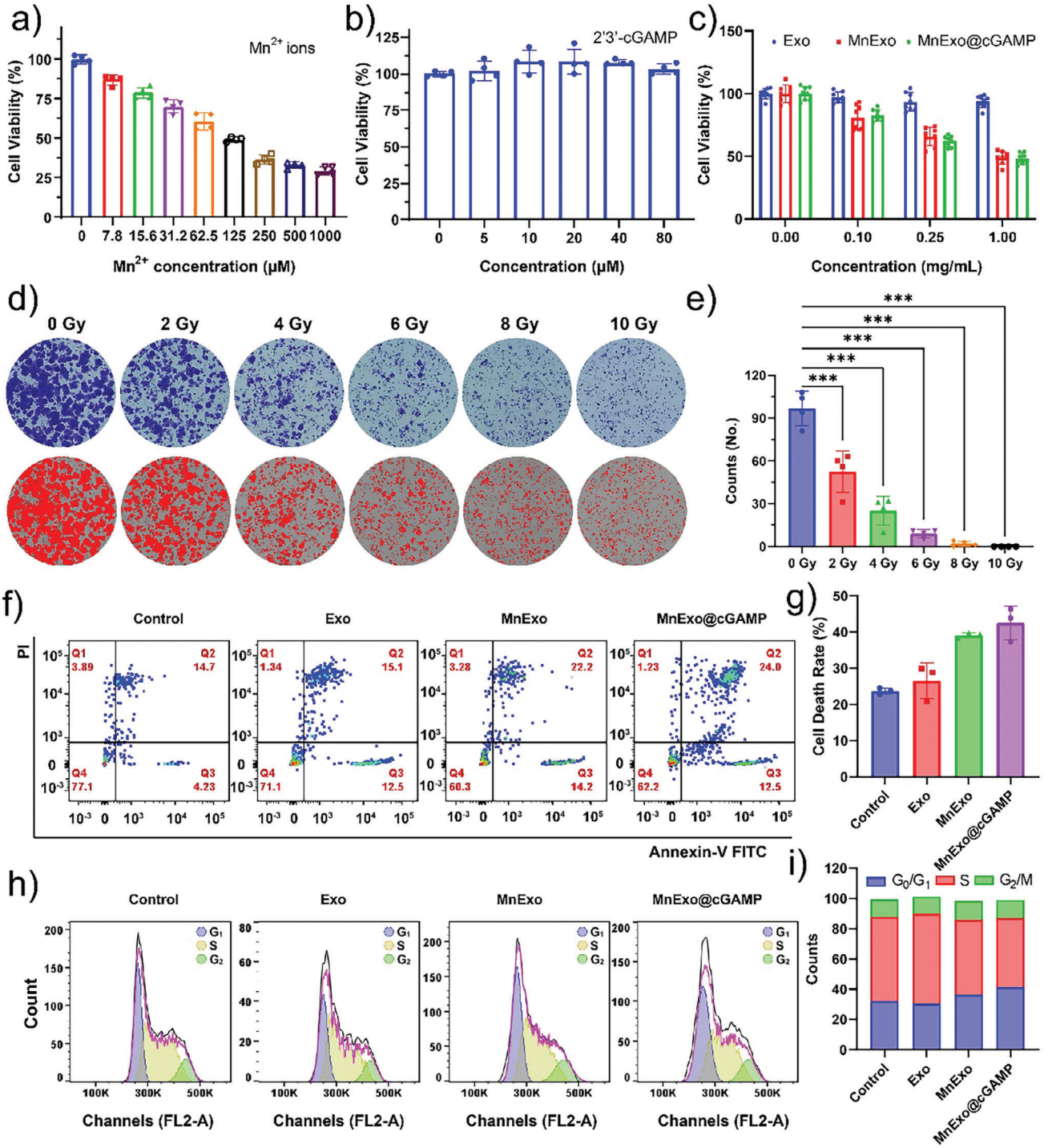

Figure 2. In vitro antitumor effect of MnExo@cGAMP and its components. a,b) Viability of B16F10 cells incubated with different concentrations of Mn^{2+} ions (a) and 2,3-cGAMP (b) for 24 h. c) Viability of B16F10 cells incubated with different concentrations of Exo, MnExo, and MnExo@cGAMP for 24 h. d,e) Colony formulation of B16F10 cells after various dose (0, 2, 4, 6, 8, 10 Gy) of X-ray irradiation (d) and the corresponding quantification (e). f,g) Apoptosis/necrosis analysis of B16F10 cells under different treatments (Control, Exo, MnExo, and MnExo@cGAMP) via flow cytometry measurement (f) and the corresponding quantification (g). h,i) Cell cycle analysis of B16F10 cells after different treatments (Control, Exo, MnExo, and MnExo@cGAMP) via flow cytometry measurement (h) and the corresponding quantification (i).

the nanoplatforms that promote DCs maturation are significant for DCs mediated specific antitumor immunotherapy. Therefore, an in vitro co-culture system based on Transwell device was established to evaluate the contribution of MnExo@cGAMP to the DCs maturation, antigen presentation, and T cell activation. As we know, apoptotic tumor cells are weak immunogenic for they will release corresponding immunostimulatory cytokines, such as high mobility group box 1 (HMGB1), calreticulin (CRT), and tumor-associated antigens (TAAs).[36] Meanwhile, Free Mn^{2+} ions will increase the sensitivity of cGAS to cytosolic dsDNA from tumor cells, and then activate the cGAS-STING pathway together with 2′,3′-cGAMP to maturate DCs.[26] As shown in **Figure 3a**, well-differentiated and immature DCs from BMDCs were co-incubated with various formulations (A1: Control, A2: 5 μM Mn^{2+} ions, A3: 20 μM 2′,3′-cGAMP, A4: 5 μM Mn^{2+} ions plus 20 μM 2′,3′-cGAMP)-treated B16F10 cells for maturation detection by dying tumor cells-original neo-antigens, Mn^{2+} ions, and 2′,3′-cGAMP. In Control group and Mn^{2+} ions group, the surface expression of CD80 and CD86 was in a low level (20.2% and 23.1%, Figure 3b,c). While the combination treatment by Mn^{2+} ions and 2′,3′-cGAMP greatly promote the DCs maturation, which was verified by higher level of CD80 and CD86 expression (87.6%, Figure 3c).

Furthermore, to evaluate the antigen presentation performance of mature DCs and T cell activation, THP-1 cells were co-incubated with mature DCs (Figure 3a). The surface expression of CD4 and CD8 protein was tested using flow cytometry to show the anti-tumor immune response.[37] According to the results, the absolute percentage of $CD8^+$ cells in combined treatment group was 26.5%, which was significantly higher in comparison with the Control group (15.7%, Figure 3d). As pro-inflammatory cytokines such as TNF-α and IL-6 secreted by mature DCs and activated T cells are critical for anti-tumor therapy,[38] the relevant concentration in medium were measured by ELISA (Figure 3e,f). Compared to the Control group, Mn^{2+} ions and/or 2′,3′-cGAMP-treated groups exhibited increased production of both TNF-α and IL-6, demonstrating that potential anti-tumor efficacy. Simultaneously, the gene expression of TNF-α and IL-6 was measured using real-time quantitative polymerase chain reaction (RT-qPCR), and the results are in consistence with the ELISA measurement (Figure 3g,h). The above results revealed that Mn^{2+} ions and/or 2′,3′-cGAMP treatments of melanoma could effectively lead to DCs maturation, antigen presentation, and T cell activation, which provided evidences for the anti-tumor immunotherapy of MnExo@cGAMP exosomes in melanoma.

2.4. In Vivo Anti-Tumor Treatment

To evaluate the in vivo anti-tumor therapeutic efficacy of as-synthesized MnExo@cGAMP, B16F10-tumor-bearing C57/BL6 mice models were established via intraperitoneal injection of tumor cells. First, we evaluated the pharmacokinetics and in vivo biodistribution of MnExo@cGAMP to test the autologous targeting performance. The elimination half-life time in blood after intravenously injection was about 18.33 min (Figure S3, Supporting Information). Meanwhile, obvious fluorescence intensity in tumor sites was detected in tumor 12 h post-injection (Figure S4, Supporting Information), demonstrating the efficient tumor accumulation and targeting activity of MnExo@cGAMP. The fluorescence intensity gradually fade 24 h later, indicating the rapid degrade in tumor tissues. The tumor bearing mice were randomly divided into six groups (n = 5): G1: Control, G2: MnExo, G3: MnExo@cGAMP, G4: RT, G5: MnExo + RT, and G6: MnExo@cGAMP + RT. The formulation was intravenously injected at days 0, 2, 4, and 6 with a concentration of 10 mg kg^{-1} (100 μL) and mice in G4, G5, and G6 groups were irradiated by X-ray (4 Gy) at days 1, 3, 5, and 7 (**Figure 4a**). Compared with the body weight in Control group, there is no conspicuous difference for MnExo and MnExo@cGAMP groups (Figure 4b), indicating the excellent biocompatibility of engineered exosomes. X-ray irradiated groups (G4, G5, and G6) displays slightly decreased body weight, which are in the normal range.[39] The change of tumor volume is an intrinsic index to evaluate the therapeutic efficacy of MnExo@cGAMP. Compared to the rapid growth rate of tumor volume in Control group, MnExo and MnExo@cGAMP exosomes treatment exhibits obvious tumor growth inhibition and the efficacy of MnExo@cGAMP is better than MnExo because of the additional 2′,3′-cGAMP (Figure 4c). Meanwhile, synchronous X-ray irradiation greatly inhibit the growth rate of tumor in MnExo +RT and MnExo@cGAMP + RT groups, demonstrating the efficient therapeutic outcome of radiotherapy on melanoma.[40] Moreover, compared to the tumor growth in RT group, the combination of RT and engineered exosomes exhibits more significant tumor growth inhibition effect, which is consistence with the speculation (Figure 4c,d).

The average tumor tissue weight and photographs (Figure 4d,e) obviously display the therapeutic difference among groups. Subsequent hematoxylin and eosin (H&E) staining of tumors in various groups revealed that treatment with MnExo@cGAMP resulted in extensive tumor cell death with few cellular nuclear staining (Figure 4f), demonstrating the recovery of normal tissues. Meanwhile, the H&E staining images of main organs (Figure S5, Supporting Information) revealed the biosafety of as-synthesized nanoagonists to normal tissues. Obvious high level of ROS in tumor tissues was detected in MnExo@cGAMP + RT group (Figure 4g, Figure S6, Supporting Information), which may attribute to X-ray irradiation and Mn^{2+} mediated biocatalysis. Increased intracellular oxidative stress could promote the immunogenic tumor cell death during treatment.[41] Therefore, we further characterize the expression of the key components of the cGAS-STING pathway in tumor cells. Western blotting showed low levels of STING and IRF3 expression in MnExo@cGAMP treated tumor compared to the Control group (Figure 4h), while phosphorylated STING (p-STING) exhibited a relative higher expression, demonstrating the successful binding between STING and cGAMP to activate cGAS-STING-IRF3 pathway.[25] The above results revealed the in vivo antitumor efficacy of MnExo@cGAMP and its ability to induce cGAS-STING pathway activation.

2.5. In Vivo Anti-Tumor Immune Response

Before evaluate the immune response after MnExo@cGAMP + RT treatment, terminal deoxynucleotidyl transferase (TdT) dUTP Nick-End Labeling (TUNEL) assay (**Figure 5a,d**) and Ki-67 assay (Figure 5b,e) were further employed to exhibit the efficient

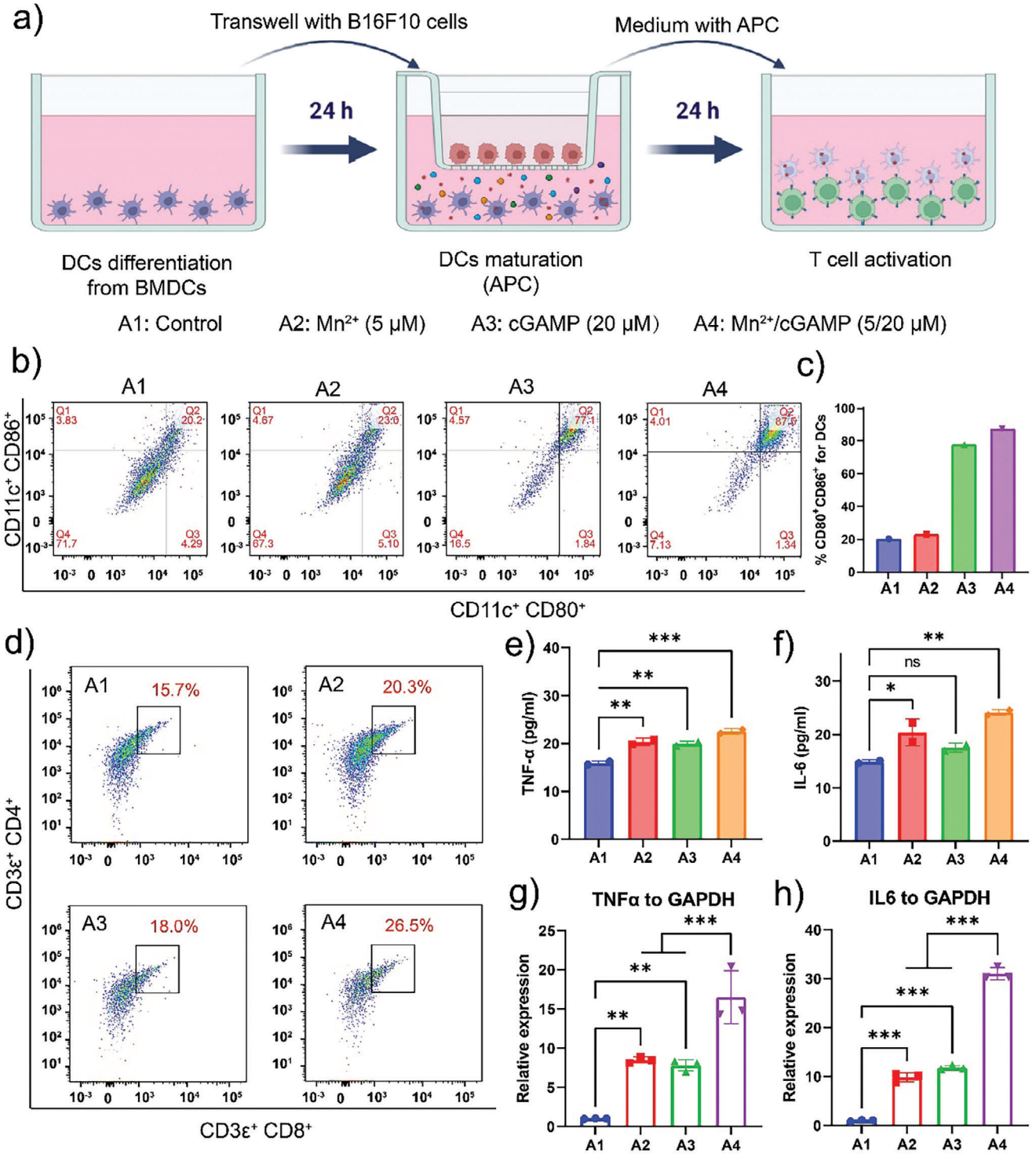

Figure 3. The DCs maturation and T cell activation after treatment with as-prepared various formulations. A1: Control, A2: 5 μM Mn^{2+}, A3: 20 μM 2,3-cGAMP, A4: 5 μM Mn^{2+} together with 20 μM 2,3-cGAMP. a) Schematic illustration of the DCs maturation and T cell activation by various treated B16F10 medium in Transwell insert plate. b,c) Representative flow cytometry plots (b) and corresponding quantification (c) of mature DCs ($CD11c^+CD86^+$) after treatments. d) Representative flow cytometry plots of T cell activation ($CD3^+CD8^+$) after treatment with APC. e,f) Pro-inflammatory cytokine TNF-α (e) and IL-6 (f) levels in DCs/T cells co-incubation supernatants via Elisa analysis. g,h) Real-time quantitative polymerase chain reaction (RT-qPCR) for the expression of TNF-α (g) and IL-6 (h).

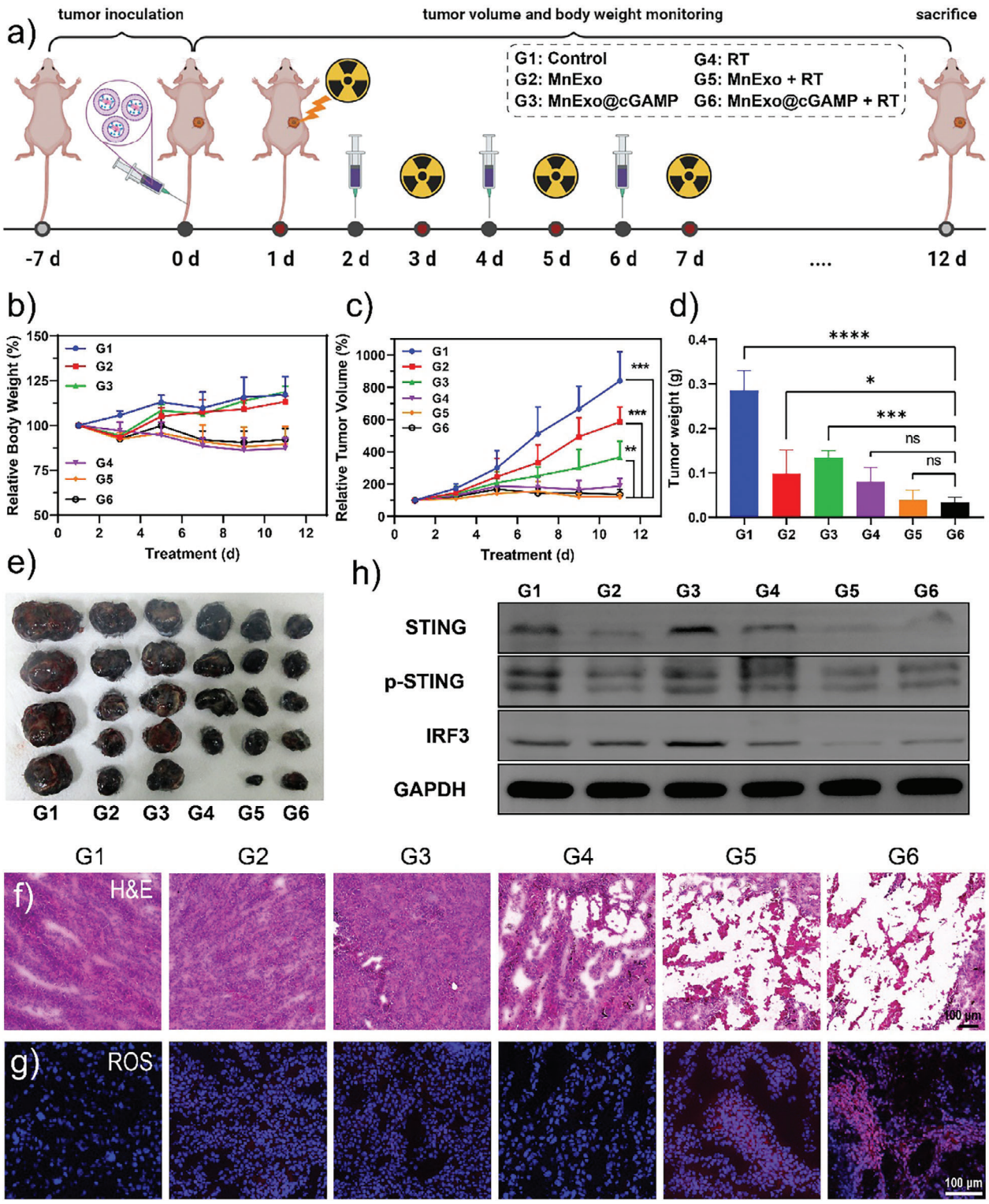

Figure 4. Antitumor effects of MnExo@cGAMP treatment on B16F10 melanoma-bearing mice. a) Schematic illustration to evaluate the antitumor therapeutic efficacy and immune response after treating with different formulations. G1: Control, G2: MnExo, G3: MnExo@cGAMP, G4: RT, G5: MnExo with RT, G6: MnExo@cGAMP with RT. b,c) The volume of tumor (b) and body weight of mice (c) in different groups in the period of 11 days' treatment. d,e) The average weight (d) and photographs (f) of tumor tissue in different groups after 11 days' treatment. f,g) H&E staining (f) and ROS staining (g) of tumor tissues in mice after various treatments. h) Western blot analysis on the expression of STING, p-STING, IRF3, and glyceraldehyde 3-phosphate dehydrogenase (GAPDH) in tumor cells after different treatments.

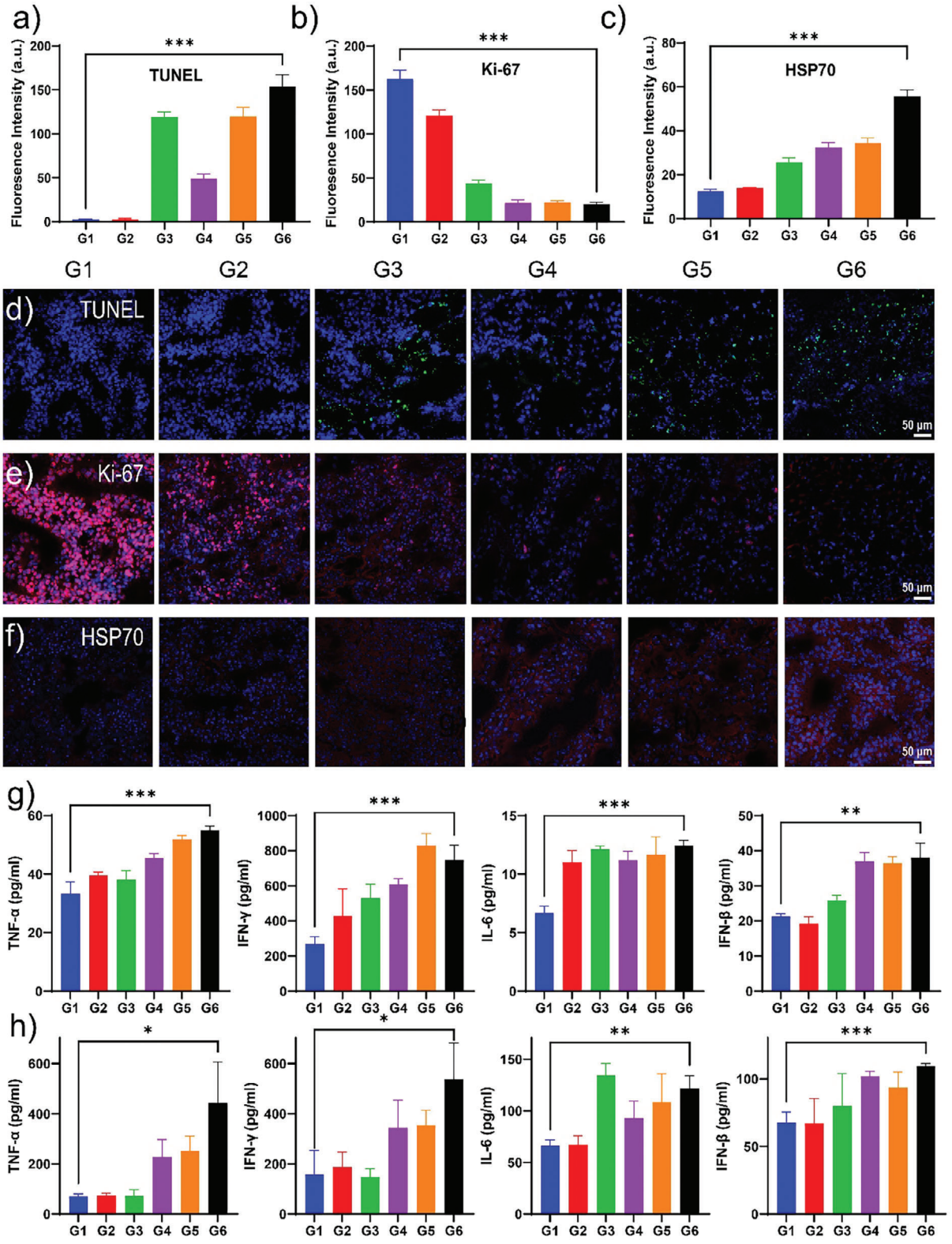

Figure 5. In vivo antitumor effect and immune response of various formulations, G1: Control, G2: MnExo, G3: MnExo@cGAMP, G4: RT, G5: MnExo with RT, G6: MnExo@cGAMP with RT. a–f) The average fluorescence intensity of TUNEL (a), Ki-67(b), and HSP70 (c) by quantitative analysis with ImageJ software and relevant fluorescence images of tumor tissues with TUNEL staining (d), Ki-67 staining (e), and HSP70 staining (f) after various treatments. g,h) The secreted level of TNF-α, IFN-γ, IL-6, and INF-β in spleen tissues (g) and tumor tissues (h) of mice after 11 days' treatment with measurement of ELISA kits.

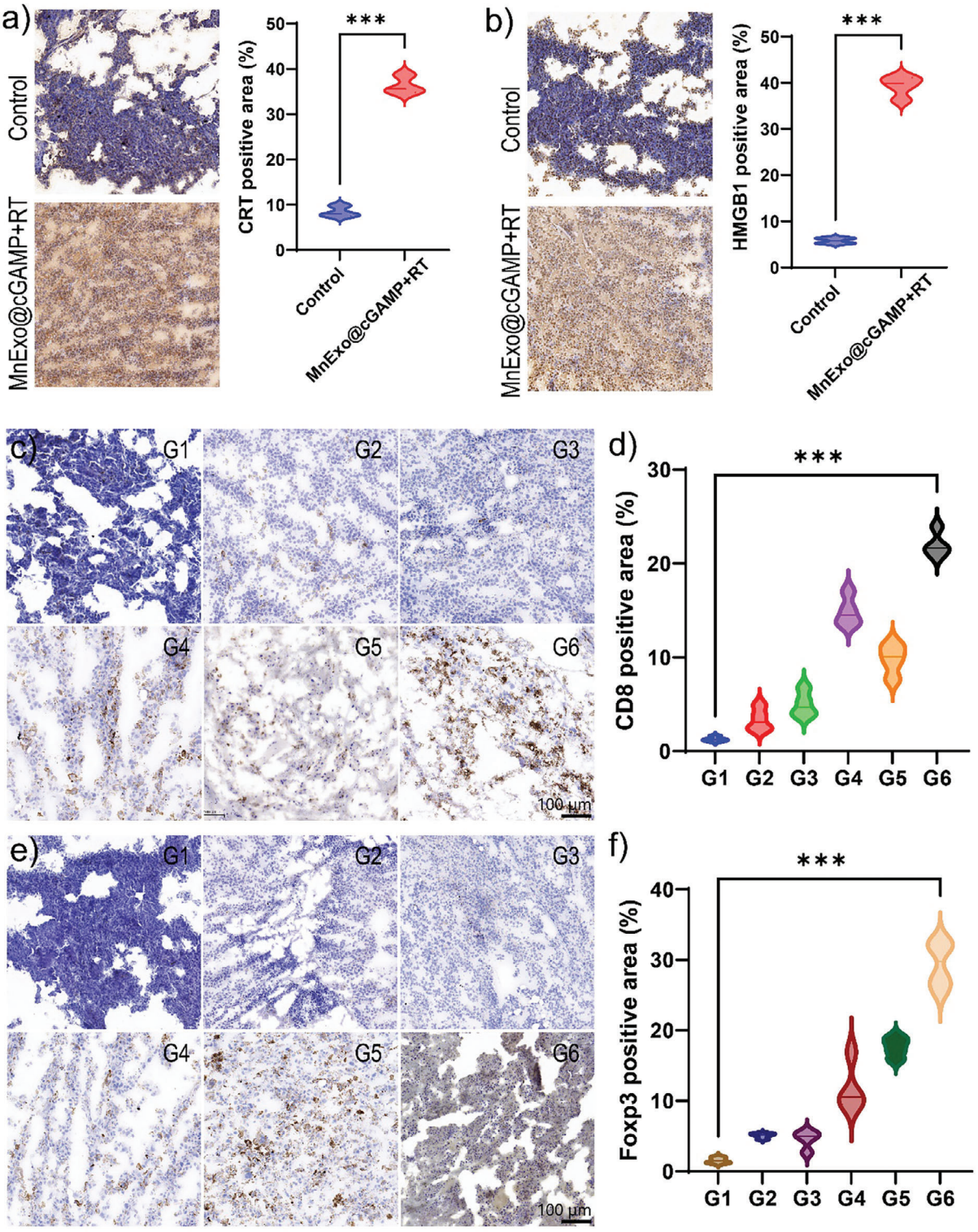

Figure 6. Immune response of MnExo@cGAMP treatment on B16F10 melanoma-bearing mice. G1: Control, G2: MnExo, G3: MnExo@cGAMP, G4: RT, G5: MnExo with RT, G6: MnExo@cGAMP with RT. a) Immunohistochemical staining and corresponding quantification of CRT in tumor tissues (Control group and MnExo@cGAMP + RT group). b) Immunohistochemical staining and corresponding quantification (k) of HMGB1 in tumor tissues (Control group and MnExo@cGAMP + RT group). c,d) Immunohistochemical staining (c) and corresponding quantification (d) of CD8 in tumor tissues of mice after different treatments. e,f) Immunohistochemical staining (e) and corresponding quantification (f) of Foxp3 in tumor tissues of mice after different treatments.

therapeutic effect in MnExo@cGAMP +RT group compared to other groups through the direct living and dead state of tumor cells after different treatments. Heat shock protein 70 (HSP70) is one an important immune regulators and triggers for MHC-I cross-presentation.[42] The staining results showed obvious up-expression in MnExo@cGAMP + RT group compared with other groups, demonstrating the efficient anti-tumor immune response (Figure 5c,f).

Cytokines mediated intercellular communication plays key role between leukocytes for immune response and inflammation.[43] Among of them, the tumor necrosis factor (TNF)-α is central in orchestrating the inflammatory immune response.[44] Therefore, the level of TNF-α in both spleen and tumor tissues was measured by ELISA (Figure 5g,h). Alone MnExo (G2) or MnExo@cGAMP (G3) exosomes treatment showed none significant change of intra-tumoral TNF-α expression compared to the Control group (G1). However, low-dose X-ray irradiation (G4) would promote the expression of TNF-α, confirming that radiotherapy is a form of immunogenic strategy. Importantly, combined therapy of MnExo@cGAMP exosomes and radiotherapy displayed highest TNF-α expression, indicating the highest immune response. Type I interferons are essential to the development of robust adaptive antitumor immunity owing to their ability to stimulate T cell cross-priming, potentially rendering tumors more susceptible to checkpoint blockade.[45] Moreover, cGAS-STING pathway is a potent driver of inflammation and promotes the transcription of genes encoding Type I interferons.[46] ELISA results (Figure 5g,h) showed the significantly increased IFN-γ expression in both MnExo + RT and MnExo@cGAMP + RT groups compared to the Control group, which is consistence with the TNF-α results. Furthermore, the significantly increased IL-6 and IFN-β confirmed the antitumor immune response after MnExo@cGAMP + RT treatments.

The production of tumor specific antigen (TSA), neoantigen processing and presentation, and T cell activation and infiltration are the key procedures for immune response after nanotherapy.[47] Immunogenic cell death (ICD) is a distinct form of RCD that is capable of triggering an adaptive immune response targeted toward damage-associated molecule patterns (DAMPs) from dying cells. Meanwhile, calreticulin (CRT) and high-mobility group box 1 (HMGB1) are two typical DAMPs of ICD.[48] The immunohistochemical staining analysis of tumor tissue after treatment showed that MnExo@cGAMP + RT treatment significantly promote the release of both CRT (**Figure 6a**) and HMGB1 (Figure 6b) compared to the Control group, revealing that the combined therapy with MnExo@cGAMP and RT are immunogenic for melanoma. Therefore, we next investigated cytotoxic T lymphocytes (CTLs) infiltration in tumor. Compared to the Control group, the number of CTLs ($CD8^+CD3^+$) slightly increased in MnExo and MnExo@cGAMP treated group (Figure 6c,d). However, additional low-dose X-ray irradiation could promote the activation and filtration of CTLs in tumor, which are explained for the high expression in both RT and MnExo + RT group (Figure 6d). Moreover, highest number of CTLs were detected in MnExo@cGAMP + RT group, demonstrating the effective immune response happened in melanoma. Meanwhile, the expression of Foxp3 (a special subset of $CD4^+$ T cells) exhibited the similar trend as CTLs in different groups (Figure 6e,f), revealing that MnExo@cGAMP + RT treatment will lead to the increase of regulatory T-cells to maintain immune homeostasis during therapy. Pulmonary metastasis is most frequently happened in melanoma due to various reasons.[49,50] The immunohistochemical staining images of lung tissues (Figure S7, Supporting Information) showed inhibited lung metastasis after various treatments because of the effective immune response.

3. Conclusion

In summary, an engineered autologous cell-derived exosomes (MnExo@cGAMP) containing metalloimmunotherapy regulator and STING agonist were successfully fabricated to boost antitumor immunity of melanoma by cascade cGAS-STING pathway activation together with radiotherapy. Taking advantage of autologous cell-derived exosome carriers, the MnExo@cGAMP system exhibited efficient loading capacity, targeted delivery performance, immune surveillance escape, and excellent biocompatibility. Traditional radiotherapy alone is hard to induce immune response even it can trigger the generation of dsNDA. However, After MnExo@cGAMP was internalized by tumor cells, the released Mn^{2+} ions will sensitize cGAS to dsDNA and also enhance STING binding, resulsting in the activation of cGAS-STING pathway together with loaded 2′,3′-cGAMP. Meanwhile, external radiation could further enhances the generation of type I IFN, which forwardly promote DCs muturation, antigen presentation, T cell activation, and final antitumor immunity. Overall, this engineered autogolous exosome exosomes based on diverse targets demonstrated an unique potential to overcome the low response rate of melanoma immunotherapy via metalloimmunotherapy combiend radiotherapy.

Supporting Information

Supporting Information is available from the Wiley Online Library or from the author.

Acknowledgements

This work was supported by the Postdoctoral Fellowship Program of CPSF (GZC20230196) and the National Natural Science Foundation of China (Nos. 21788102 and 51971116). Many thanks for the funding support by union project of BUCT-CJFH biomedical center (PT2407, 2024-NHLHCRF-YXHZ-MS-05). Zhang F. and Zhang Z. contributed equally to this work.

Conflict of Interest

The authors declare no conflict of interest.

Data Availability Statement

The data that support the findings of this study are available from the corresponding author upon reasonable request.

Keywords

autologous exosome, cGAS-STING pathway, melanoma, radio-immunotherapy

Received: September 25, 2024
Revised: November 14, 2024
Published online:

[1] W. Guo, H. Wang, C. Li, *Signal Transduction Targeted Ther.* **2021**, *6*, 316.
[2] D. Schadendorf, A. C. J. van Akkooi, C. Berking, K. G. Griewank, R. Gutzmer, A. Hauschild, A. Stang, A. Roesch, S. Ugurel, *Lancet* **2018**, *392*, 971.
[3] C. Yang, C. Tian, T. E. Hoffman, N. K. Jacobsen, S. L. Spencer, *Nat. Commun.* **2021**, *12*, 1747.
[4] B. M. Robertson, M. E. Fane, A. T. Weeraratna, V. W. Rebecca, *Nat. Cancer* **2024**, *5*, 964.
[5] W. Xie, Y. Li, Z. Guo, J. Lu, G. Li, Z. Zhang, F. Zhang, Y. Wei, X. Wang, L. Zhao, *ACS Appl. Mater. Interfaces* **2024**, *16*, 18411.
[6] Z. Guo, X. Gao, J. Lu, Y. Li, Z. Jin, A. Fahad, N. U. Pambe, H. Ejima, X. Sun, X. Wang, W. Xie, G. Zhang, L. Zhao, *ACS Nano* **2024**, *18*, 6975.
[7] M. Marzagalli, N. D. Ebelt, E. R. Manuel, *Semin. Cancer Biol.* **2019**, *59*, 236.
[8] L. Sun, J. Wu, F. Du, X. Chen, Z. J. Chen, *Science* **2013**, *339*, 786.
[9] S.-R. Woo, M. B. Fuertes, L. Corrales, S. Spranger, M. J. Furdyna, M. Y. K. Leung, R. Duggan, Y. Wang, G. N. Barber, K. A. Fitzgerald, M.-L. Alegre, T. F. Gajewski, *Immunity* **2014**, *41*, 830.
[10] W. Fang, Z. Jing, Y. Li, Z. Zhang, Z. Lin, Z. Yang, Y. Tian, C. Zhang, Y. Ma, L. Hou, F. Meng, X. Liang, X. Zhang, *Cell Rep. Phys. Sci.* **2024**, *5*, 101752.
[11] B. A. Flood, E. F. Higgs, S. Li, J. J. Luke, T. F. Gajewski, *Immunol. Rev.* **2019**, *290*, 24.
[12] K. Yang, W. Han, X. Jiang, A. Piffko, J. Bugno, C. Han, S. Li, H. Liang, Z. Xu, W. Zheng, L. Wang, J. Wang, X. Huang, J. P. Y. Ting, Y.-X. Fu, W. Lin, R. R. Weichselbaum, *Nat. Nanotechnol.* **2022**, *17*, 1322.
[13] X. Sun, Y. Zhang, J. Li, K. S. Park, K. Han, X. Zhou, Y. Xu, J. Nam, J. Xu, X. Shi, L. Wei, Y. L. Lei, J. J. Moon, *Nat. Nanotechnol.* **2021**, *16*, 1260.
[14] X. Kong, H. Zuo, H.-D. Huang, Q. Zhang, J. Chen, C. He, Y. Hu, *J. Adv. Res.* **2023**, *44*, 119.
[15] J. Wang, S. Li, M. Wang, X. Wang, S. Chen, Z. Sun, X. Ren, G. Huang, B. D. Sumer, N. Yan, Y.-X. Fu, J. Gao, *Sci. Immunol.* **2024**, *9*, eadj3945.
[16] X. Chen, F. Meng, Y. Xu, T. Li, X. Chen, H. Wang, *Nat. Commun.* **2023**, *14*, 4584.
[17] P. Dosta, A. M. Cryer, M. Z. Dion, T. Shiraishi, S. P. Langston, D. Lok, J. Wang, S. Harrison, T. Hatten, M. L. Ganno, V. A. Appleman, G. M. Taboada, N. Puigmal, S. Ferber, S. Kalash, M. Prado, A. L. Rodríguez, W. S. Kamoun, A. O. Abu-Yousif, N. Artzi, *Nat. Nanotechnol.* **2023**, *18*, 1351.
[18] Y. Wang, S. Li, M. Hu, Y. Yang, E. McCabe, L. Zhang, A. M. Withrow, J. P.-Y. Ting, R. Liu, *Nat. Nanotechnol.* **2024**, *19*, 856.
[19] I. K. Herrmann, M. J. A. Wood, G. Fuhrmann, *Nat. Nanotechnol.* **2021**, *16*, 748.
[20] H. Liu, Z. Geng, J. Su, *Extracell. Vesicles Circ. Nucleic Acids* **2022**, *3*, 63.
[21] E. I. Buzas, *Nat. Rev. Immunol.* **2023**, *23*, 236.
[22] R. Kalluri, V. S. LeBleu, *Science* **2020**, *367*, eaau6977.
[23] P. D. Robbins, A. E. Morelli, *Nat. Rev. Immunol.* **2014**, *14*, 195.
[24] P. Kurywchak, J. Tavormina, R. Kalluri, *Genome Med.* **2018**, *10*, 23.
[25] N. Samson, A. Ablasser, *Nat. Cancer* **2022**, *3*, 1452.
[26] M. Lv, M. Chen, R. Zhang, W. Zhang, C. Wang, Y. Zhang, X. Wei, Y. Guan, J. Liu, K. Feng, M. Jing, X. Wang, Y.-C. Liu, Q. Mei, W. Han, Z. Jiang, *Cell Res.* **2020**, *30*, 966.
[27] X. Wang, J. Xia, L. Yang, J. Dai, L. He, *Cancer Gene Ther.* **2023**, *30*, 1051.
[28] Y. Zhang, J. Bi, J. Huang, Y. Tang, S. Du, P. Li, *Int. J. Nanomed.* **2020**, *15*, 6917.
[29] H. Zhou, P. Yang, H. Li, L. Zhang, J. Li, T. Zhang, C. Sheng, J. Wang, *Cell Death Discovery* **2021**, *7*, 332.
[30] Y. Ren, P. Yang, C. Li, W. Wang, T. Zhang, J. Li, H. Li, C. Dong, W. Meng, H. Zhou, *Cell Death Discovery* **2023**, *9*, 267.
[31] L. Li, X. Yang, *Oxid. Med. Cell Longevity* **2018**, *2018*, 7580707.
[32] P. Chen, J. B. Bornhorst, M. Aschner, *Front. Biosci.* **2018**, *23*, 1655.
[33] W. Xie, Z. Guo, L. Zhao, Y. Wei, *Prog. Mater. Sci.* **2023**, *138*, 101145.
[34] R. Kakarla, J. Hur, Y. J. Kim, J. Kim, Y.-J. Chwae, *Exp. Mol. Med.* **2020**, *52*, 1.
[35] S. K. Wculek, F. J. Cueto, A. M. Mujal, I. Melero, M. F. Krummel, D. Sancho, *Nat. Rev. Immunol.* **2020**, *20*, 7.
[36] L. Galluzzi, A. Buqué, O. Kepp, L. Zitvogel, G. Kroemer, *Nat. Rev. Immunol.* **2017**, *17*, 97.
[37] F. Meng, Z. Lin, Y. Ma, R. Che, C. Zhang, Y. Wei, X. Song, X. Liang, X. Zhang, *Cell Rep. Phys. Sci.* **2024**, *5*, 102023.
[38] J.-L. Wautier, M.-P. Wautier, *Int. J. Mol. Sci.* **2023**, *24*, 9647.
[39] K. Wang, J. E. Tepper, *Ca-Cancer J Clin.* **2021**, *71*, 437.
[40] S. J. Rogers, E. Puric, B. Eberle, N. R. Datta, S. B. Bodis, *Dermatol. Res. Pract.* **2019**, *2019*, 9435389.
[41] J. Wan, X. Zhang, Z. Li, F. Mo, D. Tang, H. Xiao, J. Wang, G. Rong, T. Liu, *Adv. Healthcare Mater.* **2023**, *12*, 2202710.
[42] G. Sha, Z. Jiang, W. Zhang, C. Jiang, D. Wang, D. Tang, *Int. Immunopharmacol.* **2023**, *122*, 110492.
[43] G. Altan-Bonnet, R. Mukherjee, *Nat. Rev. Immunol.* **2019**, *19*, 205.
[44] G. van Loo, M. J. M. Bertrand, *Nat. Rev. Immunol.* **2023**, *23*, 289.
[45] B.-S. Pan, S. A. Perera, J. A. Piesvaux, J. P. Presland, G. K. Schroeder, J. N. Cumming, B. W. Trotter, M. D. Altman, A. V. Buevich, B. Cash, S. Cemerski, W. Chang, Y. Chen, P. J. Dandliker, G. Feng, A. Haidle, T. Henderson, J. Jewell, I. Kariv, I. Knemeyer, J. Kopinja, B. M. Lacey, J. Laskey, C. A. Lesburg, R. Liang, B. J. Long, M. Lu, Y. Ma, E. C. Minnihan, G. O'Donnell, et al., *Science* **2020**, *369*, eaba6098.
[46] Y. Liu, P. Xu, S. Rivara, C. Liu, J. Ricci, X. Ren, J. H. Hurley, A. Ablasser, *Nature* **2022**, *610*, 761.
[47] W. Xie, J. Lu, Z. Guo, X. Guo, Y. Chi, J. Ye, J. Zhang, W. Xu, L. Zhao, Y. Wei, *Nano Res.* **2022**, *15*, 2244.
[48] A. D. Garg, L. Galluzzi, L. Apetoh, T. Baert, R. B. Birge, J. M. Bravo-San Pedro, K. Breckpot, D. Brough, R. Chaurio, M. Cirone, A. Coosemans, P. G. Coulie, D. De Ruysscher, L. Dini, P. de Witte, A. M. Dudek-Peric, A. Faggioni, J. Fucikova, U. S. Gaipl, J. Golab, M.-L. Gougeon, M. R. Hamblin, A. Hemminki, M. Herrmann, J. W. Hodge, O. Kepp, G. Kroemer, D. V. Krysko, W. G. Land, F. Madeo, et al., *Front. Immunol.* **2015**, *6*, 1.
[49] J. Qin, Z. Zhang, Z. Fu, H. Ren, M. Liu, M. Qian, B. Du, *Cell Mol. Immunol.* **2020**, *17*, 1269.
[50] Y.-M. Hyun, S.-U. Seo, W. S. Choi, H.-J. Kwon, D.-Y. Kim, S. Jeong, G.-Y. Kang, E. Yi, M. Kim, H. J. Ryu, M. R. Looney, E. Y. Choi, H. S. Kim, *Sci. Adv.* **2020**, *6*, eabc4882.